Origin of resonance structures in magneto-optical spectra of InSb and $In_{1-x}Mn_xSb$

C. Thurn and V. M. Axt
Theoretische Physik III, Universität Bayreuth, D-95440 Bayreuth, Germany

A. Winter and H. Pascher
Experimentalphysik I, Universität Bayreuth, D-95440 Bayreuth, Germany

H. Krenn
Institut für Experimentalphysik, Karl-Franzens-Universität Graz, A-8010 Graz, Austria

X. Liu and J. K. Furdyna
Department of Physics, University of Notre Dame, Notre Dame, Indiana 46556, USA

T. Wojtowicz
Institute of Physics, Polish Academy of Sciences, 02-668 Warsaw, Poland
(Received 9 October 2009; published 24 November 2009)

InSb and InMnSb samples have been investigated by means of magneto-optical Kerr effect and magnetic circular dichroism. In binary semiconductor compounds such as InSb the observed magneto-optical spectra exhibit narrow and distinct resonances which can be associated with dipole-allowed transitions between the Landau levels in conduction and valence bands. With increasing magnetic field the Landau splitting increases and the observed peaks change their position and amplitude accordingly. In contrast to this observation, the magneto-optical spectra of the diluted magnetic semiconductor InMnSb show only one strong and broad resonance. Contrary to what one expects, particularly in narrow gap materials with large g factors and small effective masses, the shape and position of this resonance do not change with the applied magnetic field. It is found, however, that the amplitude depends linearly on the magnetization of the samples. In this paper we describe how these observations can be understood by means of a $\vec{k}\cdot\vec{p}$ theory incorporating the exchange interaction of free carriers with localized electrons in the Mn ions.

DOI: 10.1103/PhysRevB.80.195210 PACS number(s): 75.50.Pp, 78.20.Ls, 75.30.−m, 71.70.−d

I. INTRODUCTION

A novel concept for electronic devices, commonly referred to as "spintronics," is based on the control of spins in magnetic materials which can be achieved electrically as well as optically. Ferromagnetic semiconductors are very promising materials for the realization of spintronic devices. To use these materials effectively, however, one needs an in-depth understanding of their magnetic properties and their electronic band structure. In addition, for optical control, a detailed knowledge of the optical properties is also indispensable.

Whereas the alloy GaMnAs has already been very extensively studied[1–4] there are relatively few reports in the literature on narrow gap ferromagnetic materials such as InMnSb. Owing to the high g factor and small effective masses of the host material InSb, the Landau level and Zeeman splitting in the host material is itself quite large, and one therefore expects a stronger influence of the host band structure relative to the exchange interaction between free carriers and Mn magnetic moments than in wide gap materials. Thus, the investigation of InMnSb offers a promising perspective on understanding the magnetic interactions in ferromagnetic semiconductors.

In the present paper measurements of the magneto-optical Kerr effect (MOKE) and the magnetic circular dichroism (MCD) on ferromagnetic InMnSb samples are reported and compared with corresponding results for InSb. The most remarkable finding is the fact that there is one strong and relatively broad feature in the MOKE and MCD spectra of InMnSb, the position of which within experimental error does not depend on the external magnetic field if the magnetization is saturated, even if $\mu_0 H$ is larger than $\mu_0 M$ (H denoting the magnetic field and M denoting the magnetization). The amplitude of the feature depends only on M with no influence of H. It turns out that the experimental findings can be well understood in terms of a $\vec{k}\cdot\vec{p}$ band structure model.[5]

The paper is organized as follows: in Sec. II we describe the experimental setup used to obtain the magneto-optical spectra and the properties of InMnSb. The theoretical model used to calculate the band structure and the optical properties under the influence of magnetization and external magnetic field is described in Sec. III. A few technical details of the theoretical model will be outlined in the Appendix. In Sec. IV the actual measurements are shown and compared to calculations, followed by a discussion of the results. In a final section the pertinent conclusions to be drawn from our analysis are stated.

II. EXPERIMENTAL METHOD AND INVESTIGATED MATERIALS

A. Polar magneto-optical Kerr effect and magnetic circular dichroism

Highly doped diluted magnetic III-V semiconductors typically are ferromagnetic. In contrast to II-VI materials where

Mn^{2+} can substitute for the cations without affecting the crystal quality and the free carrier density, in III-V materials Mn^{2+} acts as an acceptor and also tends to build clusters. To optimize their properties, samples have to be grown by low-temperature molecular beam epitaxy[6,7] resulting in hole densities up to 10^{20} cm^{-3}. The high doping levels cause strong free carrier absorption and thus magneto-optical experiments using reflected light such as MOKE and MCD are advantageous for the investigation of these materials. In this paper we shall concentrate on the so-called polar MOKE, where the k vector of the incident light is oriented parallel to the magnetic field.

To understand the origin of MOKE and MCD effects in magnetic semiconductors it should be recalled that here the spin splitting of the energy bands is strongly influenced by the magnetization via the exchange interaction between the localized magnetic moments and band carriers as well as by the usual Zeeman splitting. These splittings give rise to different refractive indices for right- and left-hand circularly polarized components of the linearly polarized incident light beam (which we will refer to as σ^+ and σ^- polarizations, respectively). When the light beam is reflected from the sample surface, the two circularly polarized components suffer different phase shifts and different reflectivities. The two reflected components recombine to form an elliptically polarized beam. Owing to the different phase shifts, the main axis of polarization is then rotated with respect to the initial polarization. This can be described by Fresnel's formula for reflection of the electric field $\vec{E}$ at the interface between a medium with refractive index 1 (air) and a medium with complex refractive indices $\tilde{n}_\pm = n_\pm - i \cdot \kappa_\pm$ (the diluted magnetic semiconductor), where the "+" and "–" subscripts correspond to the σ^+ and σ^- polarizations, respectively:

$$\vec{E}_{\mathrm{refl}} = \tilde{r}_\pm \vec{E}_0 = \frac{1-\tilde{n}_\pm}{1+\tilde{n}_\pm}\vec{E}_0, \tag{1}$$

where $\tilde{r}_\pm = r_\pm \exp(i\varphi_\pm)$ is the complex reflection coefficient. From Eq. (1) we directly obtain

$$\varphi_\pm = \arctan\left(\frac{2\kappa_\pm}{1-n_\pm^2-\kappa_\pm^2}\right). \tag{2}$$

The Kerr rotation, i.e., the rotation of the plane of polarization of linearly polarized light reflected from the surface of a magnetized sample, is then calculated to be

$$\Theta_{\mathrm{Kerr}} = \frac{1}{2}(\varphi_- - \varphi_+). \tag{3}$$

The difference in the reflected intensities of the left- and right-hand circularly polarized light is defined as the MCD:

$$\mathrm{MCD} = \frac{r_+^2 - r_-^2}{r_+^2 + r_-^2}. \tag{4}$$

Figure 1 shows a schematic diagram of the experimental setup used for polar Kerr effect measurements. A halogen lamp or globar together with a grating spectrometer have been used as a tunable monochromatic light source. Behind the first polarizer P the light is polarized vertically. After passing the photoelastic modulator (PEM) the polarization vector of the light is periodically switched from vertical to horizontal polarization with a frequency of about 50 kHz (characterized as $\lambda/2$ mode, denoting that the maximum phase shift of the modulator in this case is like that of a half wave plate). The light reflected from the sample is detected after passing through the analyzer A oriented 45° away from the vertical direction. At $B=0$ kG [B denoting the flux density $B=\mu_0(H+M)$] the projections of the electric field orientations between which the modulator operates on the direction of the analyzer are equal. A lock-in amplifier that obtains its reference from the modulator and the signal from the detector measures the difference between the two projections which, as noted, is zero at $B=0$. If the sample rotates the plane of polarization, the difference between the two projections no longer vanishes and is detected by the lock-in amplifier. We refer to this signal as "DLI" (difference lock-in). A second lock-in amplifier, receiving its reference from the chopper, measures the overall intensity "SLI" (sum lock-in). From both signals the rotation angle Θ_{Kerr} of the polarization of the reflected light can be obtained by

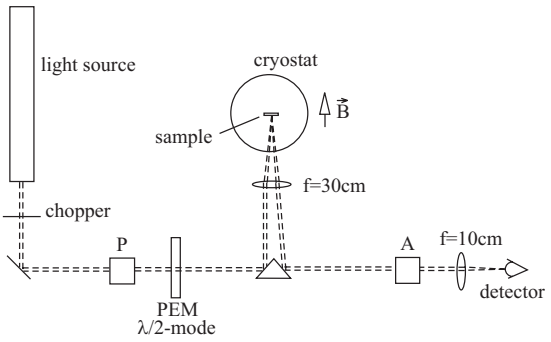

FIG. 1. Experimental setup (see text for details).

$$\Theta_{\mathrm{Kerr}} = \frac{1}{2}\arcsin\left(\frac{\frac{\mathrm{DLI}}{\mathrm{SLI}}}{I_1 - I_2\frac{\mathrm{DLI}}{\mathrm{SLI}}}\right). \tag{5}$$

The constants I_1 and I_2 can be calculated numerically from the working principle of a lock-in amplifier. However, even small misalignments of the directions of the polarizers affect these constants. Therefore, in order to improve experimental accuracy, the constants were determined from a calibration measurement. The use of a differential method makes this experimental setup highly sensitive enabling us to resolve rotations of the polarization of the reflected light with an accuracy of up to 0.002°. For the measurement of MCD, the PEM is used in the $\lambda/4$ mode and the analyzer behind the sample is removed. In this case the DLI lock-in amplifier measures the difference of the reflected intensities R_+ and R_- of the σ^+ and σ^- polarized light, and the SLI lock-in amplifier measures their sum. From both quantities the MCD can be readily obtained (J_1 is the first Bessel function):

$$\mathrm{MCD} = \left[\frac{\pi}{2}J_1\left(\frac{\pi}{2}\right)\right]^{-1}\frac{\mathrm{DLI}}{\mathrm{SLI}}. \tag{6}$$

These experiments yield the magnetic-field dependence of the magnetization if measurements are carried out at a fixed

wavelength; and at a fixed magnetic field the wavelength dependence (the spectra) of the magneto-optical effects can be recorded. Details on how to describe measurements with the PEM can be found in Refs. 8 and 9.

B. InMnSb

InSb is a III-V semiconductor with a narrow band gap of 0.235 eV at liquid helium temperature. Due to this small gap considerable interactions between valence- and conduction-band states can occur. Thus, InSb exhibits the lowest effective mass ($m_e^* \approx 0.014 m_0$) and the highest mobility of electrons in this class of materials.

As is the case for all ordinary (i.e., not magnetically doped) III-V semiconductors, InSb behaves diamagnetically. However, incorporating small amounts of Mn in the lattice results in paramagnetism. This is because the Mn ion enters the InSb lattice as Mn^{2+} ion, whose d electrons represent a half-filled shell, resulting in a vanishing orbital momentum and a spin quantum number of $\frac{5}{2}$. Therefore, the magnetization of the electron spins of the Mn ions in an external magnetic field follows a Brillouin function $B_{5/2}$. Furthermore, the lattice lacks one electron per Mn ion resulting in a high hole density in InMnSb. However, the hole density is usually lower than the Mn concentration due to large compensation effects, e.g., because some Mn ions occupy interstitial sites instead of replacing the In atoms, where they act as double donors.

As mentioned above, isolated Mn^{2+} ions act paramagnetically. The holes are able to mediate an interaction between theses ions via the so-called Ruderman-Kittel-Kasuya-Yosida (RKKY) interaction:[3] a hole spin is aligned when passing a Mn ion. While traveling through the lattice the degree of spin polarization of the holes gradually decreases. If the distance between the Mn ions is small enough so that the spin alignment of the hole can influence the spin orientation of another Mn ion, ferromagnetic interaction occurs.

$In_{1-x}Mn_xSb$ becomes ferromagnetic for $x \gtrsim 1.5\%$. Due to strongly decreasing crystal quality, homogeneous samples with concentrations greater than 3% are hard to obtain, since phase separation begins to occur as the Mn concentration increases. The carrier and the Mn density both influence the Curie temperature of InMnSb resulting in values of usually less than 20 K. It should also be noted that in ferromagnetic samples the contribution to the spin splitting caused by the exchange interaction between free carriers and the d electrons of the localized Mn ions can be much larger than the Zeeman effect of the nonmagnetic host.

Our measurements have been carried out on an InMnSb sample grown by molecular beam epitaxy (MBE). The composition of the different layers comprising the sample was controlled by the atomic flux during the growth process, as follows. On top of a 0.5-mm-thick GaAs (001) substrate we grew a 400 nm CdTe layer, followed by a 180 nm layer of low-temperature InSb and a 230 nm layer of InMnSb, also grown at low temperature, with a Mn concentration $x = 1.5\%$ ($n_{\mathrm{Mn}} = 2.2 \times 10^{20}$ cm^{-3}). The concentration of free carriers was estimated from Hall effect measurements to be $p = 1.5 \times 10^{20}$ cm^{-3}, and magnetization data obtained by a superconducting quantum interference device magnetometer indicate a magnetization of $M_S = 10.6 \times 10^3$ A/m at saturation ($\mu_0 M_S = 0.133$ kG). We shall compare below our results for InMnSb with measurements on pure InSb that have been performed using a 1.52-mm-thick InSb wafer available commercially.

III. CALCULATION OF BAND STRUCTURE AND DIPOLE TRANSITIONS

In order to describe the optical properties of InMnSb, we use a standard $\vec{k} \cdot \vec{p}$ approach to characterize the electronic structure. Our model accounts for the two lowest spin-split conduction bands and six valence bands (the heavy hole, the light hole, and the split-off band), which are mixed by an 8×8 Luttinger Hamiltonian in a flux density $\vec{B}$ (the so-called Pidgeon-Brown Hamiltonian $H_{\mathrm{P\&B}}$ extended for finite wave vectors $\vec{k}$).[5] Due to the small band gap of InMnSb, mixing between the conduction and the valence bands is rather strong. The external field gives rise to a Zeeman splitting of the Mn spin states:

$$H_{\text{Mn-Zeeman}} = g_{\mathrm{Mn}} \mu_B \sum_n \vec{S}_n \cdot \vec{B}, \tag{7}$$

where $g_{\mathrm{Mn}} = 2$ is the g factor of Mn ions, $\vec{S}_n$ is the spin operator of the nth Mn atom, and μ_B is the Bohr magneton. In Mn-doped samples hybridization effects between the localized d shells of the Mn ions and the itinerant carriers lead to an exchange interaction, which is treated within the virtual crystal and mean-field approximations. This results in the following contribution to the Hamiltonian:

$$H_{s\text{-}pd} = x N_0 \sum_n \langle \vec{S} \rangle (\alpha \vec{s}_n^{\,s} + \beta \vec{s}_n^{\,p}), \tag{8}$$

where x is the Mn concentration, N_0 is the number of cations per volume, $\langle \vec{S} \rangle$ is the thermal expectation value for a Mn spin, and $\vec{s}_n^{\,s/p}$ stands for the nth electron spin operator for s-like conduction-band states or p-like valence-band states, respectively. α and β denote the corresponding exchange integrals. For magnetic fields used in the present paper, the magnetization is in most cases nearly saturated, and the mean-field ansatz certainly holds. We have taken the direction of the equilibrium magnetization as the z direction, which is also the direction of the external magnetic field, thus, replacing the spin operators in Eq. (8) by their z components. Further details, including the explicit form of the Hamiltonian, can be found in Ref. 5 (see also Ref. 10 of the present paper). The above contributions define our system Hamiltonian H_{sys}. In addition, the dipole coupling to an external light field $\vec{E}$ is taken into account in the usual way:

$$H_{\mathrm{int}} = -\vec{E} \cdot \vec{P}, \tag{9}$$

where $\vec{P}$ denotes the polarization operator. In order to calculate the optical response we first determine the eigenstates $|\nu\rangle$ and eigenvalues E_ν of H_{sys} by direct diagonalization as described in Ref. 5. The eigenstates $|\nu\rangle$ are conveniently labeled by a two-dimensional vector $\vec{k}$ with components

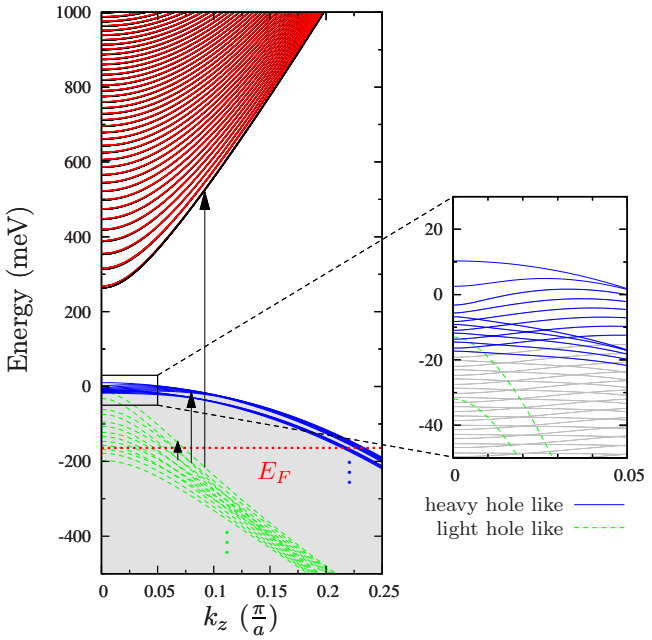

FIG. 2. (Color online) Band structure of $In_{0.985}Mn_{0.015}Sb$ in an external magnetic field of 80 kG and saturated magnetization at a temperature $T=1.8$ K. a denotes the lattice constant.

(k_y,k_z) and a discrete index j, which results from the diagonalization of H_{sys} for a given $\vec{k}$. A state of given j contains superpositions involving up to four consecutive Landau quantum numbers and is referred to as Landau level in what follows. We adopt the Landau gauge, where the energies are degenerate with respect to k_y. For right-hand (σ^+) or left-hand (σ^-) circularly polarized light we obtain a complex linear optical susceptibility which is a scalar and can be written as

$$\chi_{\pm}(\omega) = \sum_{j,j',\vec{k}} \frac{[f_j(k_z) - f_{j'}(k_z)]|M_{jj'}^{(\pm)}(\vec{k})|^2}{\varepsilon_0 V[E_j(k_z) - E_{j'}(k_z) - \hbar(\omega + i\gamma)]} + \chi_\infty, \tag{10}$$

where $f_j(k_z)$ is the thermal occupation of a state with given values of (j,k_z), V denotes the volume, γ is a phenomenological damping constant which provides a finite width for each transition, and χ_∞ stands for the high-frequency background susceptibility. Finally, $M_{jj'}^{(\pm)}(\vec{k})$ are the $\sigma^\pm$ components of the transition dipole matrix elements. Details of their calculation can be found in the Appendix.

Figure 2 shows the calculated band structure of InMnSb as a function of the field-parallel component k_z of the vector $\vec{k}$ for an external magnetic field of 80 kG where the magnetization is saturated. The conduction band breaks up into well separated Landau levels which are further split by the Zeeman and exchange contributions. For the valence bands the situation is a bit more complicated due to strong band mixing effects. Nevertheless, it is possible to distinguish three classes of subbands according to whether the heavy or light hole or split-off character is dominant. Owing to their large effective masses, the heavy-hole-like subbands indicated by the gray background color in Fig. 2 are closely spaced. The solid lines display the heavy-hole-like subbands corresponding to the lowest few Landau levels. The light-hole-like subbands are spaced less densely. Again, only those subbands corresponding to the lowest few Landau levels are shown explicitly (dashed lines). The split-off-like subbands do not appear in Fig. 2. On the right-hand side a magnified view of the subbands near the band edge is depicted. It is clearly seen that many crossings between different subbands take place.

For the optical response the position of the Fermi energy is important. In our calculation we use the experimental estimates for p and n_{Mn} discussed in the previous subsection to determine the Fermi energy E_F, which is indicated by the dotted horizontal line in Fig. 2. For InSb without Mn doping the Fermi energy lies in the band gap, and therefore all valence bands are occupied.

According to Eq. (10) all transitions with nonvanishing dipole matrix elements and nonzero occupation differences $f_j(k_z)-f_{j'}(k_z)$ contribute to the susceptibility. It should be noted that the MCD and MOKE signals are affected by both the real and the imaginary part of $\chi(\omega)$. Thus, transitions whose frequencies deviate by a large detuning $\Delta\omega$ from the light frequency ω may also noticeably influence the signal, because the real part of $\chi(\omega)$ decays only as $\sim 1/\Delta\omega$. The possible contributions can be roughly classified in three categories. For both InSb and InMnSb, interband transitions (IBTs) between a valence and a conduction band may take place. Transitions involving just the valence bands occur only in the Mn-doped samples, since all final states are occupied in the intrinsic case. These intra-valence-band transitions (IVBTs) can be further subdivided according to whether both subbands originate from the same or from different types of valence subbands (heavy, light, and split-off). We account for the usual selection rules which are summarized in detail in the Appendix. The number of signal contributions is greatly restricted by the fact that, in order to yield a nonvanishing dipole matrix element, the superpositions representing the two eigenstates must contain states with Landau quantum numbers that differ at most by 1. Typical examples for the three categories of allowed transitions are depicted by arrows in Fig. 2.

IV. RESULTS AND DISCUSSION

Measurements on pure InSb have been performed at a temperature of 1.8 K. Figure 3 compares the Kerr and MCD spectra observed at 45 kG with the calculated spectra obtained using the Luttinger parameters from Ref. 11. As can be seen, there is excellent agreement between the experiment and the model calculations obtained without any adjustable parameters.

The narrow minima and maxima in Fig. 3 can be associated with left- and right-hand circularly polarized transitions between different Landau levels in the valence and the conduction band. According to the Pidgeon-Brown model[12] for interband transitions only the vicinity of the Γ point has to be considered in the calculation. Due to the low carrier concentration the Fermi energy is located within the energy gap, which means that there are no blocked interband transitions.

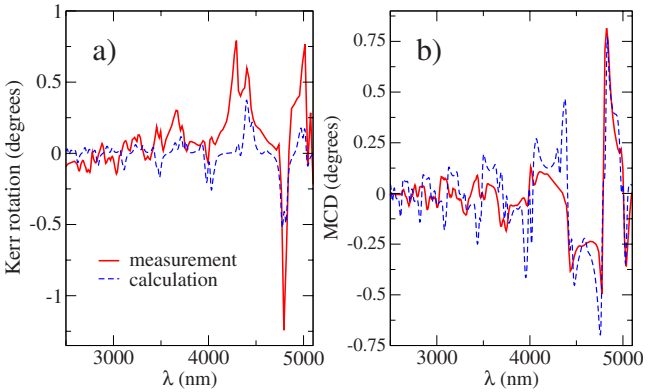

FIG. 3. (Color online) (a) Magneto-optical Kerr rotation and (b) MCD spectra for InSb at $\mu_0 H = 45$ kG and $T = 1.8$ K.

This is obvious, because the first maxima and minima in the experimental spectra occur very close to the energy gap.

Figure 4 shows the MCD spectra of pure InSb for two different external magnetic fields (15 kG and 45 kG, shifted 0.5° down and up, respectively, for clarity). Measured as well as calculated spectra are shown, and the two straight lines indicate the spectral shifts of two minima with increasing field. The variation in the spectra with external magnetic field is exactly as expected: the resonances are narrow, and their positions shift and their amplitudes increase with increasing field. This can be readily seen by observing the changes in the band structure especially the increasing Landau splitting.

Contrary to this, the diluted magnetic semiconductor InMnSb exhibits only one rather broad resonance in the magneto-optical spectra as can be seen in Fig. 5. Superimposed on this resonance is an oscillation with a comparatively small amplitude which is due to Fabry-Perot-like interferences. Such interferences show up in multilayer samples because light that has been reflected at an interface between layers can interfere with light reflected at the sample surface. In our numerical simulation we account for this ef-

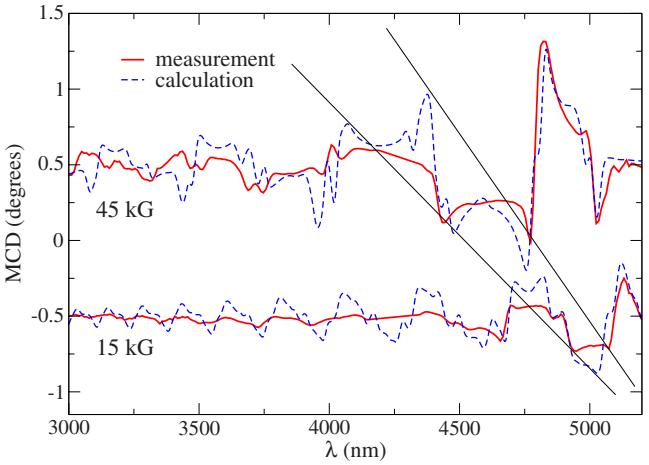

FIG. 4. (Color online) MCD spectra for InSb at $T = 1.8$ K for two different magnetic fields $\mu_0 H$ (the upper spectra have been shifted upward by 0.5° and the lower spectra have been shifted down by the same amount).

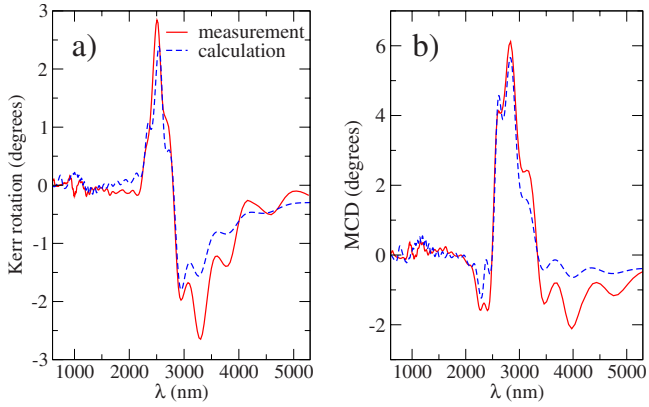

FIG. 5. (Color online) (a) Magneto-optical Kerr rotation and (b) MCD spectra for $In_{0.985}Mn_{0.015}Sb$ at $\mu_0 H = 4.5$ kG and $T = 1.8$ K.

fect by means of a transfer-matrix method.[13] In this way an excellent agreement between measurement and calculation is obtained using the model discussed in Sec. III.

In addition to the striking difference of the spectra for pure InSb and for InMnSb, the influence of the magnetic field on the spectra is also qualitatively different. In order to illustrate this aspect, we have performed calculations of MOKE spectra for different magnetic fields in the regime where the magnetization is saturated. The results are shown in Fig. 6(a). As can be seen, changing the field from 30 to 60 kG has practically no effect on the Kerr rotation. In particular, in contrast to pure InSb there is absolutely no shift of the spectral positions with changing magnetic field. *Nota bene*: due to the small concentrations of Mn ions in our samples, the value of $\mu_0 H$ can easily exceed the value of $\mu_0 M$, and despite this fact the spectra do not change with increasing field after the magnetization has been saturated. Also the amplitude is almost constant after the magnetization is saturated, as can be seen from the inset of Fig. 6(a), where we have plotted the maximum value of the MOKE spectrum as a function of magnetic field. This behavior is confirmed by

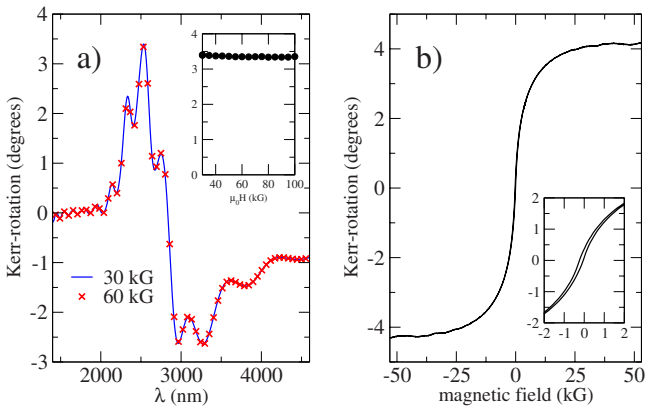

FIG. 6. (Color online) (a) Calculated Kerr spectrum of InMnSb for different $\mu_0 H$ in the regime of saturated magnetization at $T = 1.8$ K; the inset shows the maximum amplitude of the Kerr spectrum as a function of $\mu_0 H$. (b) Measured Kerr rotation angle of InMnSb for the fixed wavelength $\lambda = 3200$ nm as a function of $\mu_0 H$ at $T = 1.8$ K; the inset shows a magnified section of this hysteresis curve.

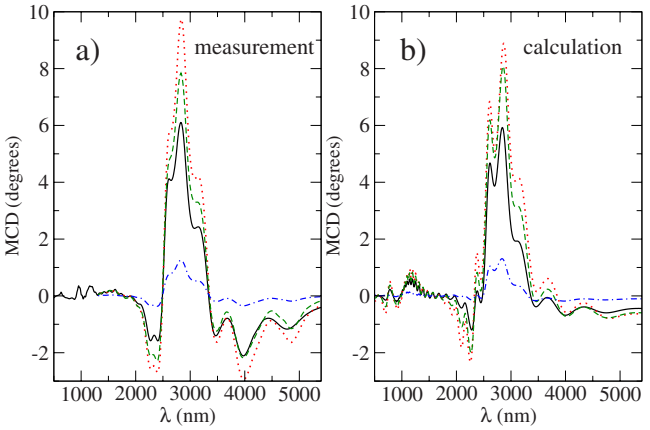

FIG. 7. (Color online) MCD spectra of InMnSb: (a) measured at different temperatures and magnetic fields [from top to bottom at 3000 nm: (1.8 K; 53 kG), (10 K; 53 kG), (1.8 K; 4.5 kG), and (10 K; 4.5 kG)], (b) calculated for corresponding magnetizations, $T=1.8$ K, $\mu_0 H=53$ kG (see text for details).

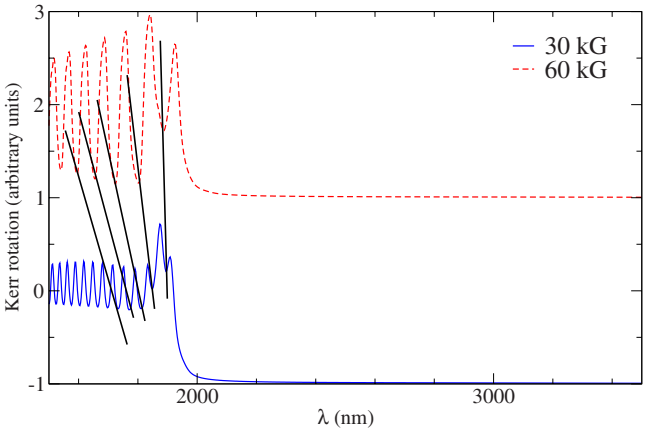

FIG. 8. (Color online) Calculated interband contribution to the magneto-optical Kerr rotation in InMnSb where inter-valence-band transitions have been switched off by hand. The curves correspond to magnetic fields $\mu_0 H$ as indicated and $T=1.8$ K (again the spectra have been shifted upward/downward by 1 unit for clarity).

the experiment. Figure 6(b) displays the Kerr rotation angle as a function of magnetic field at a fixed wavelength of 3290 nm and a temperature of 1.8 K. For fields above 30 kG the Kerr angle is indeed nearly constant. The general shape indicates that the Kerr angle is proportional to the magnetization exhibiting a hysteresis (see inset) and resembling a Brillouin function.

These findings suggest that the magneto-optical signals from our Mn-doped samples depend essentially only on the magnetization M. To further analyze this issue we have measured MCD spectra for different temperatures T and magnetic fields H. The results can be seen in Fig. 7(a). Both changes in T and H have little influence on the shape of the spectra. No shifts occur in the entire range of H, starting from low values up to fields deep in the regime where the magnetization is saturated. Only the amplitude is affected by T or H. The latter behavior is well in line with the above assumption that the T and H dependences of magneto-optical signals predominantly reflect the corresponding dependences of M. Of course, the changes in T or H have important consequences besides the variation in M; e.g., the occupations and energies of the hole states depend on T and H. In order to demonstrate that the observed behavior is mainly due to changes in M, we performed calculations where we have varied M by hand as an independent parameter. All other parameters have been kept fixed at their values corresponding to $T=1.8$ K and $\mu_0 H=53$ kG. To obtain a meaningful comparison with the experimental curves in Fig. 7(a) we have adjusted the values of M according to the measured hysteresis curves. As can be seen from the results in Fig. 7(b) all the pertinent features of the experiment are well reproduced by this procedure. In particular, the signal amplitude essentially depends linearly on the magnetization.

To understand these qualitatively different findings, it is instructive to analyze the relative contributions to the magneto-optical signal of the IBTs between the valence and the conduction band, and of the IVBTs between the light- and heavy-hole-like subbands. For InMnSb, the Fermi energy lies deep in the valence band as can be seen in Fig. 2. This gives rise to a large number of allowed IVBTs, which have nonzero dipole matrix elements due to strong band mixing effects, while only IBTs are allowed in intrinsic InSb. In order to evaluate the influence of the IBTs in InMnSb, we have calculated MOKE spectra where the IVBTs have been switched off by hand, and only the IBTs have been taken into account. The corresponding results are shown in Fig. 8. These signals are qualitatively very different from the results of the full calculation as well as from the experiment. As in InSb, these spectra exhibit several distinct and relatively sharp peaks for $\lambda \lesssim 2000$ nm, which shift with increasing magnetic fields and are zero in the spectral range where the observed spectra from InMnSb show predominant features. Clearly these features arise from IVBTs between the light- and the heavy-hole-like subbands rather than from IBTs. The reason for their predominant character is that the combined density of states is much larger for the IVBTs than for the IBTs. Thus, the IBTs are negligible compared to transitions between the valence subbands. Indeed, the results of the full calculation are practically unchanged when the IBTs are left out (curves not shown). It is only for wavelengths shorter than 2000 nm that the selection rules between different Landau levels prohibit transitions between the light- and the heavy-hole-like subbands, so IBTs can be observed in that energy domain.

Comparing the absolute signal strengths of the full calculation with Fig. 8 it may be surprising that the IBTs alone would lead to clearly visible structures in the spectral range $\lambda \lesssim 2000$ nm, i.e., in the range where in Fig. 5 only marginal features are seen. However, it should be noted that the various contributions entering the signal are not additive [cf. Eq. (2)]. In particular, strong off-resonant transitions between valence subbands tend to reduce the signal amplitude in the spectral range where the IBTs exhibit their characteristic structures and thus suppress these IBT features.

The fact that the spectra for InMnSb are dominated by IVBTs has several implications. While the peaks in InSb can be identified with single Landau levels in the conduction band, the predominant peaks in the MOKE and MCD spectra

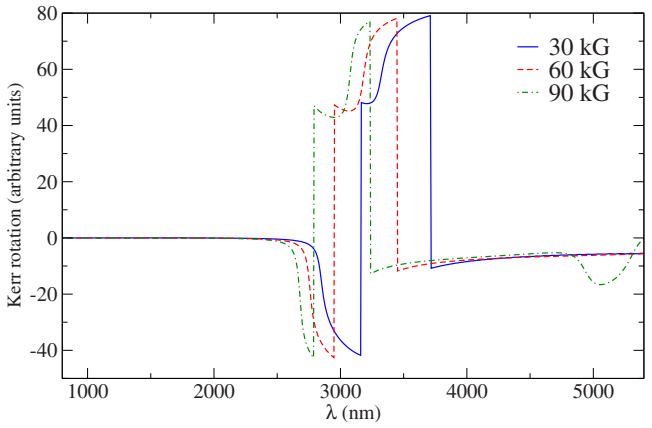

FIG. 9. (Color online) Calculated magneto-optical Kerr rotation in InMnSb that would arise solely from transitions between two pairs of spin-split light- and heavy-hole-like subbands at three different magnetic fields at $T=1.8$ K.

in InMnSb consist of a superposition of a large number of transitions between Landau levels of the light and the heavy hole type. The precise number of Landau levels involved depends on the magnetic field and in our calculations is in the range between several hundred at high fields up to 1400 at low fields. These levels are closely spaced and considerably broadened by a high scattering rate as well as a high defect density. Thus, the discrete nature of individual transitions is lost. The magnetic-field independence of the spectra is also a consequence of the dominance of IVBTs. Since all hole Landau levels are shifted in the same direction with increasing magnetic field, it is to be expected that the transition energies depend only weakly on the magnetic field compared to the IBTs. However, this fact by itself cannot explain the magnetic-field independence. In order to illustrate this point we have calculated the MOKE spectrum that would result from two isolated pairs of spin-split light- and heavy-hole-like subbands. Figure 9 shows that the corresponding curves still exhibit a slight sensitivity to the magnetic field. It is only after the superposing of all intra-valence-band transitions that the magnetic-field dependence is finally averaged out.

The spin splitting of valence-band states is dominated by the exchange interaction described by Eq. (8). This effect causes the amplitude of the signature to depend on the magnetization rather than on the external magnetic field. We note in passing that the absolute values of the amplitudes in Fig. 9 are even higher than in the full calculation where the presence of all other transitions reduces the signal as explained before.

From the above discussion it is evident that the conduction-band exchange parameter $N_0\alpha$ cannot be extracted from the experimental data, since IVBTs dominate the spectra. On the other hand, the valence-band exchange parameter $N_0\beta$ enters the signal noticeably. As the Mn spin expectation value is multiplied by the prefactor $N_0\beta$ in the exchange Hamiltonian [cf. Eq. (8)], a different value of $N_0\beta$ is equivalent to a different magnetization and therefore leads to a corresponding linear dependence of the signal amplitudes, without affecting the shape or position of the curves. Within our model we can thus use $N_0\beta$ as a fitting parameter in order to reproduce the measured amplitudes. Thorough investigations of the relation between simulations and measured data by modifying the relevant parameters over broad ranges yield the best fit for $|N_0\beta|=(2.1\pm0.4)$ eV, where the errors have been estimated from a mean square fitting procedure.

Dietl *et al.*[3] mention a well confirmed trend concerning the valence-band exchange parameter $N_0\beta$, namely, β remains constant in the case of II-VI-based diluted magnetic semiconductors, so that $N_0\beta$ decreases with increasing lattice constant. By assuming this trend to also hold for III-V semiconductors, and by taking β of GaMnAs to be (-1.2 ± 0.2) eV, they have been able to obtain reasonable estimates for the Curie temperatures for different materials (although they do not mention InMnSb). Using their assumptions the value of $N_0\beta$ for InMnSb should be between -0.66 and -0.93 eV and thus well below our best fit. On the other hand, a similar fit that we have performed for an InMnAs sample yields $N_0\beta\approx1.0$ eV in accordance with the above trend and with independent measurements.[3,5]

However, numerical tests indicate that in our model the amplitude of the spectra is noticeably affected by off-resonant transitions at large values of k_z. In this regime the accuracy of the $\vec{k}\cdot\vec{p}$ model already reaches its limits. Thus, a quantitative extraction of $N_0\beta$ is afflicted with significant uncertainties. Further investigations are therefore required to decide whether $N_0\beta$ is really larger than expected or whether the $\vec{k}\cdot\vec{p}$ model overestimates this parameter. Yet it should be stressed that these uncertainties resulting from limitations of the $\vec{k}\cdot\vec{p}$ model at large k_z values affect only the signal amplitudes. Importantly, these uncertainties have practically no effect on the shape and position of the spectra, and thus all pertinent conclusions drawn from our analysis rely only on features arising from the k_z range where the $\vec{k}\cdot\vec{p}$ model is valid.

V. CONCLUSION

In the narrow gap ferromagnetic III-V-based compound InMnSb the dominating transitions governing the electronic contribution to the dielectric function are intra-valence-band transitions from light to heavy holes. Thus, in the MOKE and MCD signals only the value of the valence-band exchange constant $N_0\beta$ enters the amplitude linearly, while the influence of the conduction-band exchange parameter $N_0\alpha$ is not noticeable.

Transitions between individual Landau levels are not distinguishable in the spectra observed on InMnSb, which instead manifest one broad signature peak. The position of this peak depends on the Fermi energy, and the magnitude of the signature—apart from the effect of $N_0\beta$—depends on the magnetization of the sample. All experimental findings are well described by the $\vec{k}\cdot\vec{p}$ model developed by Sanders *et al.*[5] In particular, the dominance of intra-valence-band transitions explains why the spectra are insensitive to external magnetic fields. Since heavy and light hole bands shift in the same direction with changing magnetic field the influence of the field strength on the corresponding transition energies is

weak. The remaining dependence of these energies does not result in measurable shifts in the spectra because the observed broad signature is a superposition of several hundred transitions between different Landau levels, forming in effect a magnetic-field-independent envelope. Finally, the dominant influence of the exchange interaction on the spin splittings in the valence bands explains the linear dependence of the signal amplitudes on the magnetization.

APPENDIX: DIPOLE MATRIX ELEMENTS

For the understanding of the optical response of any material one needs to know the dipole matrix elements $\langle \nu | M^{(\pm)} | \nu' \rangle = -e \langle \nu | r_x \pm i r_y | \nu' \rangle$ between the eigenstates of the system Hamiltonian H_{sys}. Here, e denotes the electron charge. In the approach of Ref. 5 the eigenstates $|\nu\rangle$ are represented as linear combinations of basis states $|\xi, \vec{k}, n\rangle$, where ξ specifies one of the eight bands (heavy, light, split-off, conduction, each with two possible values for the magnetic quantum number m_z), n denotes the Landau quantum number and $\vec{k}$ is a two-dimensional wave vector with components (k_y, k_z). For each $\vec{k}$ at most eight of these states are combined with up to four different consecutive values of n. Thus, $\langle \nu | \vec{r} | \nu' \rangle$ can be calculated as a linear combination of the matrix elements $\langle \xi, \vec{k}, n | \vec{r} | \xi', \vec{k}', n' \rangle$ between the basis states. For these the usual selection rules apply,

$$\langle \xi, \vec{k}, n | \vec{r} | \xi', \vec{k}', n' \rangle = \delta_{\vec{k},\vec{k}'} \delta_{n,n'} \langle u^0_\xi | \vec{r} | u^0_{\xi'} \rangle + \delta_{\xi,\xi'} \langle \varphi_{\vec{k},n} | \vec{r} | \varphi_{\vec{k}',n'} \rangle, \tag{A1}$$

where u^0_ξ is the lattice periodic part of the Bloch function from band ξ at the Γ point and $\varphi_{\vec{k},n}$ denotes the envelope function corresponding to the quantum numbers $(\vec{k}, n)$. It is known that the second term in Eq. (A1) is only a small correction to the first and thus may be neglected.[5] The neglected term would give rise to transitions with $n - n' = \pm 1$.

For interband transitions that connect a valence subband with a conduction subband it is common to use the following relation:

$$\langle \nu | \vec{r} | \nu' \rangle = \frac{i\hbar}{m_0} \frac{\langle \nu | \vec{p} | \nu' \rangle}{E_{\nu'} - E_\nu}, \tag{A2}$$

where $\vec{p}$ is the momentum operator and m_0 is the bare electron mass. For this model the matrix $-i\hbar / m_0 \langle \nu | \vec{p} | \nu' \rangle$ is given explicitly in the appendix of Ref. 5. It is easy to show that Eq. (A2) is a strict identity for the eigenstates of the semiconductor Hamiltonian without the $\vec{k} \cdot \vec{p}$ expansion at zero magnetic field. Within the $\vec{k} \cdot \vec{p}$ approach Eq. (A2) provides a simple way to account for k dependences of $\langle \nu | \vec{r} | \nu' \rangle$ beyond the k-dependent coefficients in the superposition of the basis states $|\xi, \vec{k}, n\rangle$. For the interband transitions this transformation yields dipole matrix elements that, as expected, decrease with increasing transition energies. When $\langle \nu | \vec{r} | \nu' \rangle$ is evaluated directly in the $\vec{k} \cdot \vec{p}$ theory without using this transformation, then the latter feature is lost, because the eigenfunctions are given in first-order perturbation theory with respect to k. Thus, the effect of the transformation Eq. (A2) is to provide a natural energy cutoff.

However, for transitions between valence subbands the use of this transformation becomes problematic. Here, due to the frequent crossings of subbands, many transitions with zero or nearly zero transition frequencies strongly contribute to the dielectric function. In the $\vec{k} \cdot \vec{p}$ model such low frequency transitions artificially lead to divergences in the right-hand side of Eq. (A2). To avoid these divergences we evaluate $\langle \nu | \vec{r} | \nu' \rangle$ directly by using the eigenstates of the $\vec{k} \cdot \vec{p}$ theory for IVBTs. Anyway, the main advantage of using the transformation Eq. (A2) for the IBTs is the introduction of an effective energy cutoff for the dipole matrix elements. For IVBTs this aspect is of minor importance because these transitions have a natural cutoff for two reasons. First, a k_z cutoff is imposed by the Fermi energy, since for values of k_z larger than the intersection point of the uppermost valence subband and the Fermi level all valence-band states are occupied (cf. Fig. 2). Thus, no transitions are possible for larger k_z. Second, the first term on the right-hand side of Eq. (A1) implies the selection rule $n = n'$. Thus, transitions from states with $n > \max(n')$ to unoccupied states are prohibited, where n' denotes an unoccupied valence-band state.

In conclusion, for IVBTs we prefer the direct evaluation of the dipole matrix elements according to Eq. (A1) which is not plagued by divergence problems and has a natural energy cutoff. In contrast, for IBTs the use of the transformation Eq. (A2) is well established and known to be reliable. Consequently, for IBTs we calculate the dipole matrix elements according to Eq. (A2).

[1] H. Ohno, D. Chiba, F. Matsukura, T. Omiya, E. Abe, T. Dietl, Y. Ohno, and K. Ohtani, Nature (London) **408**, 944 (2000).

[2] H. Ohno, A. Shen, F. Matsukura, A. Oiwa, A. Endo, and S. Kutsumotu, Appl. Phys. Lett. **69**, 363 (1996).

[3] T. Dietl, H. Ohno, F. Matsukura, J. Cibert, and D. Ferrand, Science **287**, 1019 (2000).

[4] T. Dietl, H. Ohno, and F. Matsukura, Phys. Rev. B **63**, 195205 (2001).

[5] G. D. Sanders, Y. Sun, F. V. Kyrychenko, C. J. Stanton, G. A. Khodaparast, M. A. Zudov, J. Kono, Y. H. Matsuda, N. Miura, and H. Munekata, Phys. Rev. B **68**, 165205 (2003).

[6] T. Wojtowicz, J. K. Furdyna, X. Liu, K. M. Yu, and W. Walukiewicz, Physica E **25**, 171 (2004).

[7] T. Wojtowicz, W. L. Lim, X. Liu, G. Cywiński, M. Kutrowski, L. V. Titova, K. Yee, M. Dobrowolska, J. K. Furdyna, K. M. Yu, W. Walukiewicz, G. B. Kim, M. Cheon, X. Chen, S. M. Wang, H. Luo, I. Vurgaftman, and J. R. Meyer, Physica E **20**, 325 (2004).

[8] J. Cerne, D. C. Schmadel, L. B. Rigal, and H. D. Drew, Rev. Sci. Instrum. **74**, 4755 (2003).

[9] Z. J. Yang and M. R. Scheinfein, J. Appl. Phys. **74**, 6810 (1993).

[10] Note: in Appendix A of Ref. 5 the Landau matrices contain several typing errors, which can be easily corrected by using Eqs.

(7)–(10) and (27) of Ref. 5. Also the bottom right entry of matrix (23) of Ref. 5 should read $\beta/6$, as can be seen in Ref. 14.

[11] I. Vurgaftman, J. R. Meyer, and L. R. Ram-Mohan, J. Appl. Phys. **89**, 5815 (2001).

[12] C. R. Pidgeon and R. N. Brown, Phys. Rev. **146**, 575 (1966).

[13] R. Nies and F. R. Kessler, Phys. Status Solidi A **111**, 639 (1989).

[14] J. K. Furdyna and J. Kossut, *Semiconductors and Semimetals, Diluted Magnetic Semiconductors*, Semiconductors and Semimetals Vol. 25 (Academic Press, Inc., New York, 1988).